DOI: 10.53469/jpce.2025.07(08).03

Multi-Temporal UAV Photogrammetry and DEM Differencing for Landslide Deformation Monitoring in a Mining Area, Inner Mongolia

Jiayi Hu[1,*], Chen Cao[1,2]

[1]College of Construction Engineering, Jilin University, Changchun 130026, Jilin, China
[2]State Key Laboratory of Deep Earth Exploration and Imaging, Changchun 130026, Jilin, China
[1]jyhu23@mails.jlu.edu.cn, [2]ccao@jlu.edu.cn.
**Correspondence Author*

Abstract: ***This study investigates slope deformation in Baiyinhu No. 2 open-pit mine (Inner Mongolia Plateau) using multi-temporal UAV photogrammetric surveys conducted in June and September 2024. High-resolution full-frame imagery (GSD ~6.3 cm) and precise POS data (GNSS/IMU, horizontal ±3 cm, vertical ±5 cm) were processed in Pix4D Mapper to generate orthoimages and DEMs. Model re-projection error (~0.1 px), point cloud density (512 pts/m²), and GCP-based RMSE (horizontal 0.091 m, vertical 0.080 m) demonstrate robust geometric accuracy. DEM differencing revealed localized subsidence up to ~0.9 m at the midsection and toe of the landslide. Additional analysis of four deformation bodies (April–September 2023) showed vertical displacements of 0.2–0.6 m. The observed deformation patterns are structurally controlled, aligning with bedding and fault orientation. UAV-based monitoring significantly reduces cost (~70% per point) and enables centimeter to decimeter detection of micro-deformation, providing a reliable basis for slope stability assessment in mining areas. The methodology offering an effective framework for deformation mapping and hazard evaluation.***

Keywords: Mining area, UAV photogrammetry, deformation monitoring.

1. Introduction

Landslides and slope deformations are among the most frequent geological hazards affecting mining areas, posing substantial risks to infrastructure, operations, and personnel (Kolapo et al., 2022, Strzałkowski et al., 2025). Effective deformation monitoring enables timely hazard assessment, early warning, and informed mitigation, thereby enhancing safety and operational continuity (Kumari et al., 2025). Remote sensing technologies, with their capacity for non-intrusive, high-resolution data acquisition over difficult terrain, have become indispensable in modern slope stability monitoring (Le Roux et al., 2025).

In recent years, Unmanned Aerial Vehicles (UAVs) have been increasingly applied in slope monitoring due to their high flexibility and spatial resolution. Turner et al. (Turner et al., 2012) demonstrated the use of UAV photogrammetry for detecting landslide displacements at centimeter-scale accuracy, while Lucieer et al. (Lucieer et al., 2014a) applied UAV-derived orthophotos to map small-scale surface movements in natural slopes. These studies suggest UAVs are particularly effective for monitoring inaccessible mining slopes.

Among UAV-based approaches, Digital Elevation Model (DEM) differencing is a straightforward and widely used method. Lucieer et al. (Lucieer et al., 2014b) successfully used multi-temporal UAV DEMs to quantify volumetric changes in a slow-moving landslide in Tasmania. Similarly, Niethammer et al. (Niethammer et al., 2012) applied DEM of Difference (DoD) analysis to assess mass wasting processes in Alpine landslides. These examples confirm that DEM differencing provides valuable information for detecting elevation changes and deformation patterns.

Despite its advantages, DEM differencing accuracy depends on survey conditions and data processing. James et al. (James et al., 2017) reported vertical accuracies of UAV photogrammetry DEMs ranging from 0.1–0.4 m under controlled surveys. Ground control points (GCPs) and stable reference surfaces are commonly applied to minimize errors and ensure reliable interpretation. Thus, while uncertainties remain, the method is robust enough for deformation detection in mining environments.

Based on this background, this study applies UAV photogrammetry and DEM differencing to evaluate the surface deformation of the mining-area slope. By comparing two UAV surveys, we aim to quantify deformation magnitudes, identify spatial patterns, and interpret possible causes related to mining activity. This research provides a practical case study of UAV-based monitoring for slope stability assessment in mining regions.

2. Study Area

The BYH coalfield is located on the southeastern margin of the Inner Mongolia Plateau, in the transitional zone between the southern segment of the western slope of the Greater Khingan Range and the Xilinhot volcanic passive continental margin. The geographic coordinates of the coalfield extend from 118°15′E to 118°40′E and 44°40′N to 45°00′N (Figure 1a). The regional landform is dominated by low mountains and hills, with elevations ranging from 835 to 1957 m. The terrain generally slopes from southeast to northwest, and valley incision exceeds 200 m in depth. The exposed strata belong to the Lower Cretaceous Damoguaihe Formation (K_1d^3), consisting mainly of interbedded mudstone, sandy mudstone, and fine- to medium-grained sandstone, with intercalations of carbonaceous mudstone and thick coal seams.

The average thickness of coal-bearing strata is about 288.27 m.

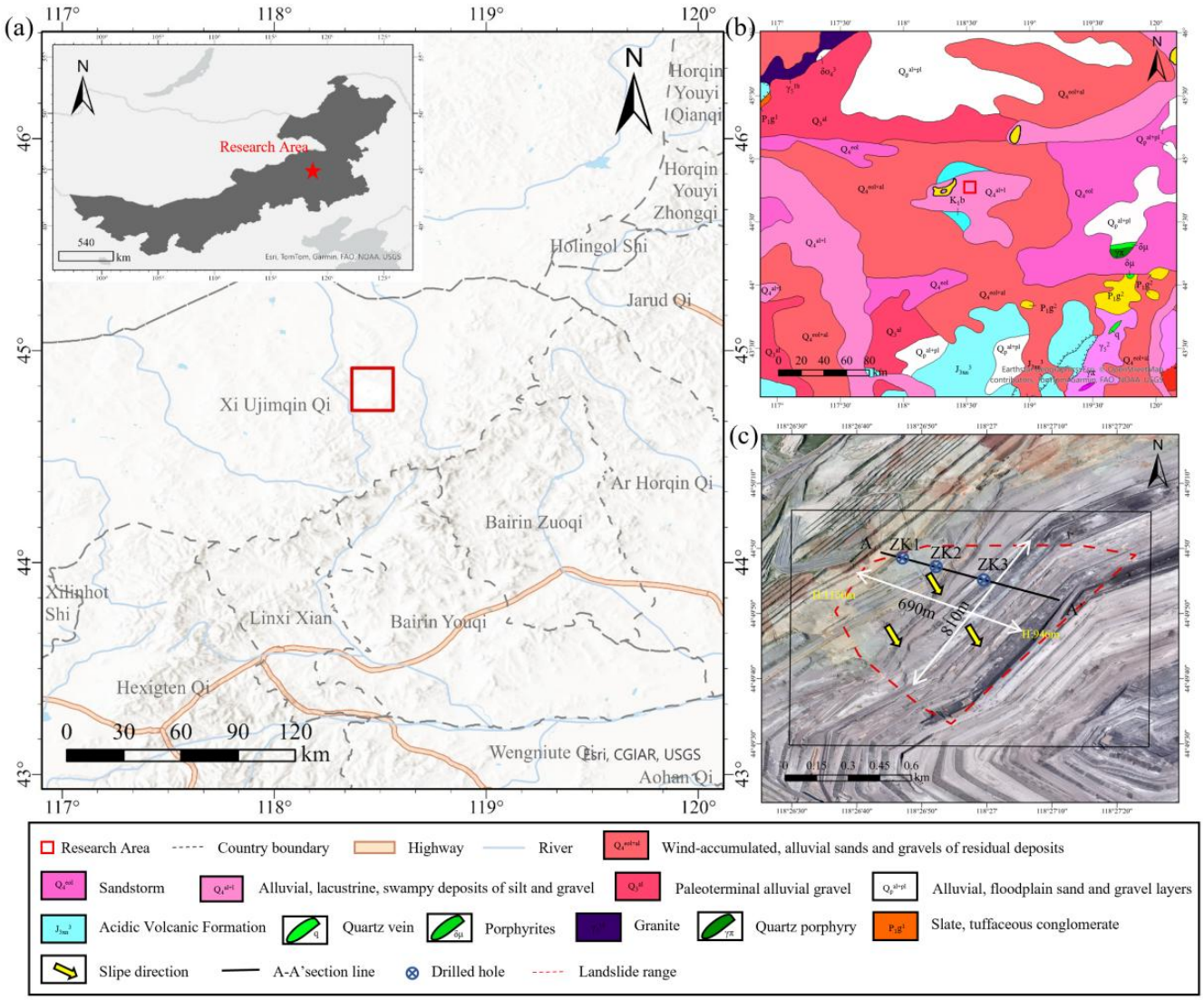

Figure 1: Regional overview of the study area (a) Geographic location of the study area; (b) Geologic map of the study area; (c) Plan view of the landslide

The BYH No. 2 open-pit mine is situated in the south-central part of the coalfield, on the northwestern limb of the BYH syncline. The strata generally dip 125°–130° with gentle angles of 5°–15°, but multi-phase tectonic activity has led to local undulations and secondary faults (Figure 1b). Seismic activity is relatively frequent in the area, with a peak ground acceleration of 0.05 g corresponding to seismic intensity VI. A magnitude 5.9 earthquake occurred in 2004, posing a potential threat to slope stability.

The landslide investigated in this study is located on the middle to upper section of the northern slope of the No. 2 open-pit mine, with coordinates ranging from 118°25′E to 118°30′E and 44°48′N to 44°52′N. The slope exhibits a stepped morphology, with elevations between 1032 m and 1101 m and a relative relief of 68.8 m, dipping from northeast to southwest. The landslide body is tongue-shaped, approximately 690 m in length and 810 m in width, covering an area of about 0.49 km². Continuous arcuate tension cracks are developed at the rear, while the toe directly borders the mining operation area, where clear shear-sliding traces can be observed (Figure 1c).

Field investigations show three prominent arcuate cracks at the landslide head, with spacing of 20–50 m, a maximum aperture of 1.2 m, and lengths exceeding 200 m. Feather-like shear cracks trending NE50° intersect the main sliding direction in the middle portion of the landslide. At the toe, step-like dislocations are evident, with a maximum vertical offset of 2.3 m, accompanied by local bulging of rock masses (Figure 1a). Stratigraphically, the landslide body is composed from top to bottom of Quaternary alluvial-proluvial sand (Q), Neogene red clay (N_2), and Cretaceous Damoguaihe Formation mudstone (K_1d^3) (Figure 1b). Weak layers are concentrated within the roof and floor of Coal Seam No. 2-1, with thicknesses ranging from 3.3 to 32.1 m. The carbonaceous mudstone exhibits extremely low shear strength (cohesion C = 3.5–6.7 kPa, friction angle φ = 6.1°–6.6°). Along cross-section PM1, three boreholes (ZK1, ZK2, ZK3) revealed sliding surfaces at elevations of 1005 m, 976 m, and 959 m, respectively, with sliding directions consistent with the bedding dip (SE125°).

3. Data and Methods

3.1 UAV Image Acquisition

In this study, a FEIMA ROBOTICS CM2600 quad-rotor UAV was employed for aerial surveying, equipped with a high-resolution full-frame camera (sensor size 25.4 mm × 16.933 mm, effective pixels 6144 × 4096). The camera was carefully calibrated, with a focal length of 28 mm, aperture f/5.6, exposure time 1/1250 s, and ISO-147. The flight altitude was set to 150 m, with a forward overlap of 80% and side overlap of 70%, ensuring sufficient image redundancy for 3D reconstruction and precise photogrammetric processing. Flight paths were automatically planned using Pix4D Capture in a serpentine pattern, covering the northern slope of the study area over 7.68 km². Each flight lasted approximately 45 minutes. The first survey was conducted on June 25, 2024, capturing 1846 oblique images, while the second survey was conducted on September 26, 2024, capturing 1271 oblique images.

3.2 Image Preprocessing and Geometric Correction

During image acquisition, high-precision POS data were simultaneously recorded using a GNSS/IMU integrated navigation system, with horizontal positioning accuracy of ±3 cm and vertical accuracy of ±5 cm. Camera distortion parameters (radial distortion coefficient $k_1 = 0.011$, tangential distortion coefficient $p_1 = 0.026$) were used to correct lens distortions. Geometric and radiometric corrections were performed in Pix4D Mapper to remove lens distortions and atmospheric scattering effects. The original ground sampling distance (GSD) of the images was 6.29 cm. After radiometric correction, the image grayscale dynamic range was expanded to 12 bits, significantly enhancing the detail resolution in shadowed and overexposed areas.

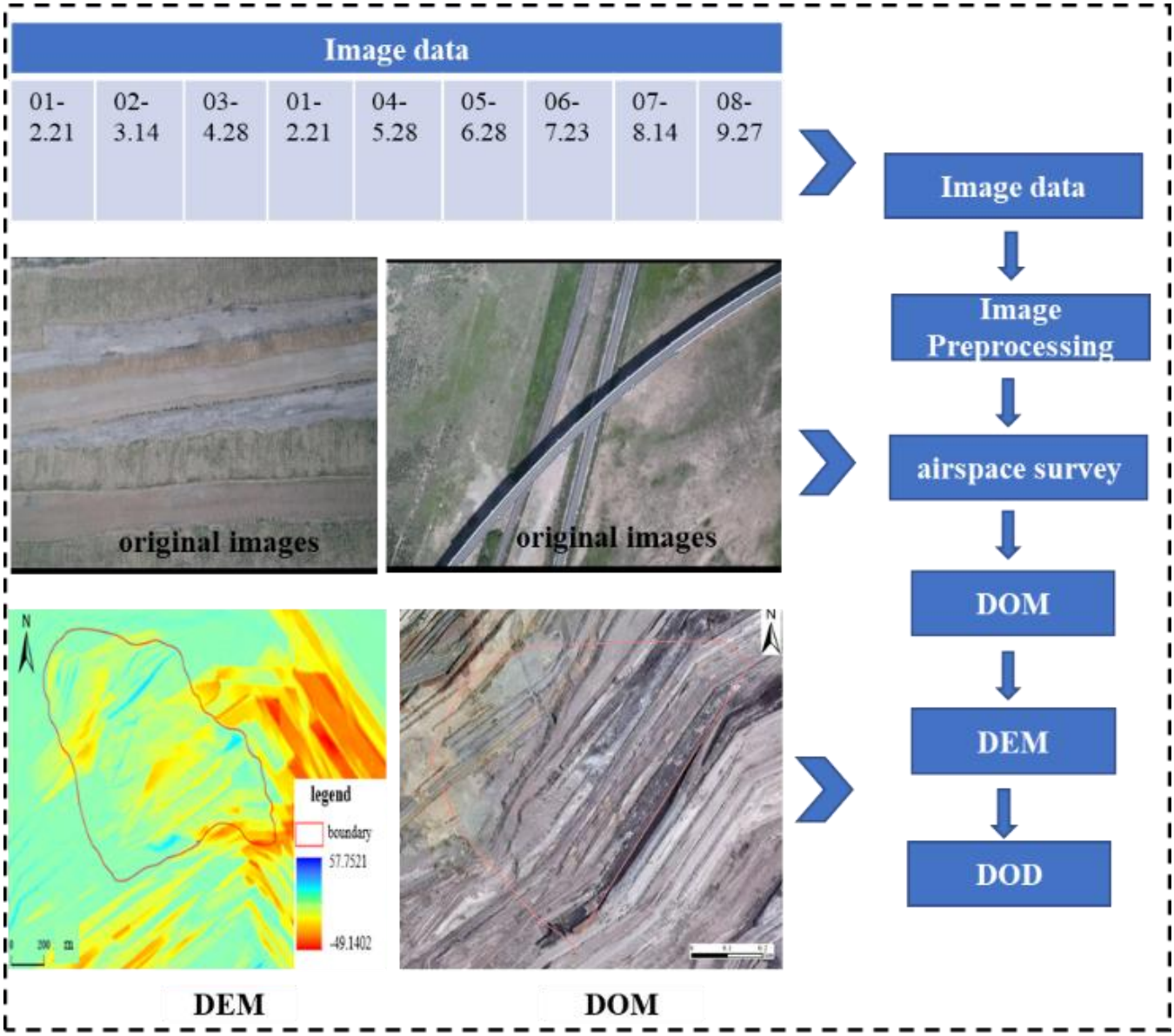

Figure 2: Technical Flowchart.

3.3 3D Modeling and Accuracy Assessment

Aerial triangulation and point cloud generation were performed in Pix4D Mapper. The results show a mean re-projection error of 0.103 pixels and a point cloud density of 512 points/m², with a median of 59,459 key points in the 3D reconstruction. After camera parameter optimization, the focal length was adjusted from 30.238 mm to 30.292 mm, and the principal point coordinates (x, y) shifted from (3107.320, 2062.420) pixels to (3107.569, 2064.552) pixels, representing

only a 0.17% change, indicating high model stability. Ground control point (GCP) validation yielded a horizontal RMSE of 0.091 m and a vertical RMSE of 0.080 m, meeting the accuracy requirements for landslide deformation monitoring.

3.4 Data Products and Applications

Two sets of orthoimages and digital elevation models (DEMs) were generated for the study area corresponding to the two survey dates (Figure 4). The datasets achieve centimeter-level horizontal accuracy, with horizontal displacement sensitivity of approximately 0.3 pixels (~1.8 cm) and vertical deformation detection limits better than 0.5 m. Compared with conventional ground-based monitoring, UAV surveying significantly reduces costs (about 70% savings per monitoring point) while providing high-resolution spatial coverage. These data form a reliable basis for subsequent 3D landslide deformation field inversion and slope stability analysis, supporting both scientific investigation and engineering management in the mining area.

4. Results

4.1 Landslide Deformation Analysis

Figure 3a and 3b present the orthophotos of the study landslide acquired on June 25, 2024, and September 26, 2024, respectively. The landslide body exhibits a tongue-shaped geometry with a clearly defined boundary, extending approximately 690 m in length and 810 m in width. Surface features, including arcuate tension cracks at the head and shear traces at the toe, are visible in both orthophotos. The slope exhibits a stepped morphology consistent with field surveys. Arrows in Figure 3a indicate the main sliding direction, highlighting zones of differential displacement.

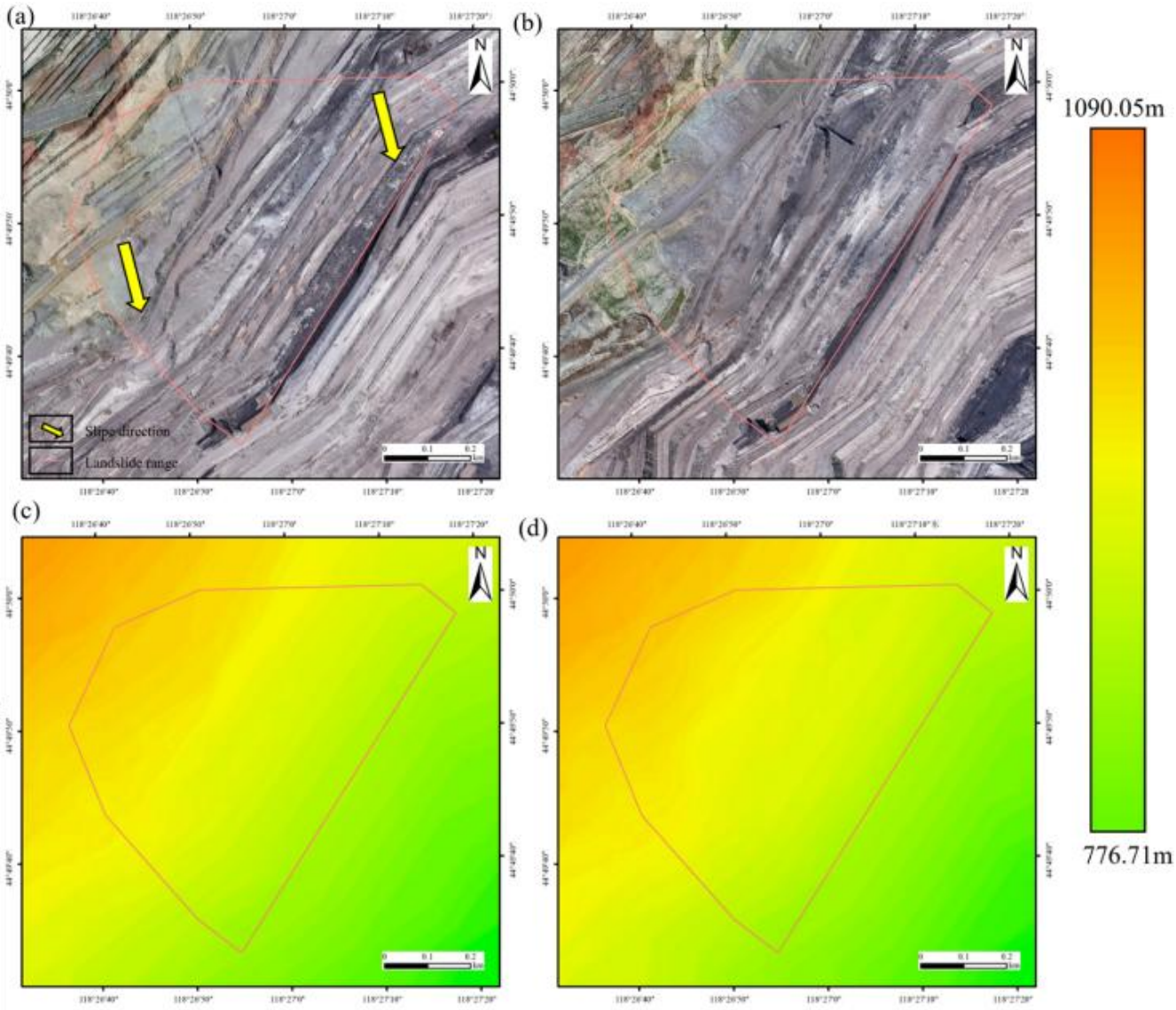

Figure 3: UAV orthophotos, DEM maps. (a) and (b) are orthophotographs from Phase I (2024.6.25) and Phase II (2024.9.26), respectively; (c) and (d) are DEM maps from Phase I and Phase II, respectively.

The corresponding DEMs (Figure 3c and 3d) reveal elevation variations ranging from 776.7 m to 1090.1 m. Visual comparison indicates localized subsidence along the midsection and toe of the landslide, consistent with observed shear zones. The vertical displacement difference map between June and September 2024 (Figure 4) further confirms areas of significant downward movement, with maximum subsidence reaching approximately 0.9 m. The distribution of vertical deformation is in agreement with the orientation of geological bedding and fault structures, suggesting that the

observed movement is structurally controlled.

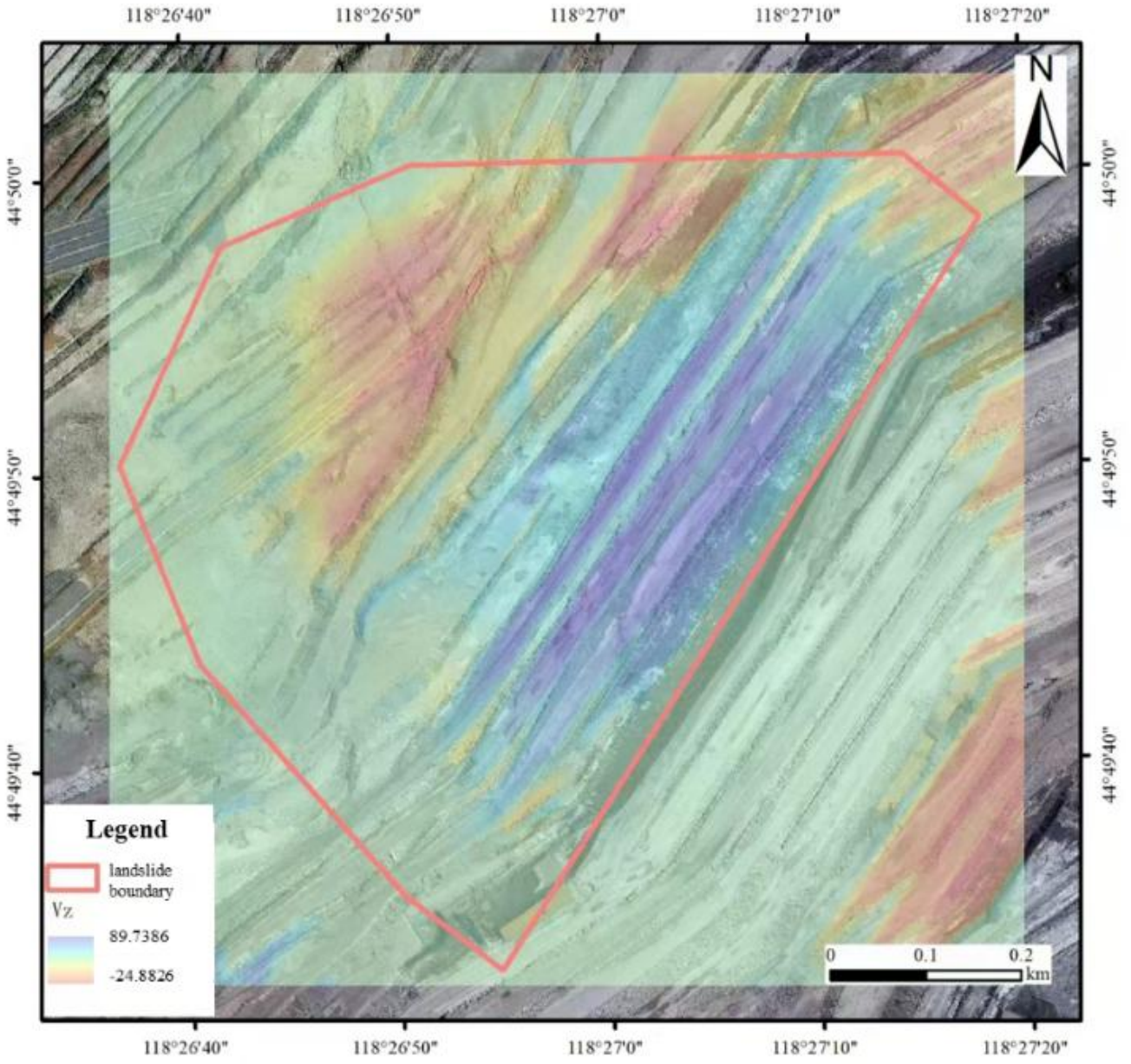

Figure 4: Digital Elevation Model of Difference (DoD) for the 2024 landslide

4.2 Deformation Body Analysis

The DoD analysis for the four deformation bodies identified in 2023 is presented in Figure 4. Significant vertical deformation is observed across all four bodies, though the magnitude and spatial pattern vary. Deformation Body 1 shows pronounced subsidence in its central and lower sections, with a maximum subsidence exceeding -1.2 m. Deformation Body 2 exhibits substantial subsidence concentrated along a linear feature, potentially related to a specific geological structure or mining influence, with max values around -0.8 m. Deformation Body 3 displays less intense but areally extensive subsidence, max ~ -0.5 m. Deformation Body 4 shows a complex pattern with zones of both subsidence (max ~ -0.7 m) and localized uplift (max ~ +0.3 m), possibly indicating different processes or material redistribution. The variation in deformation magnitude and pattern among these bodies highlights the influence of factors such as slope aspect, underlying lithology, structural geology, and proximity to mining activities.

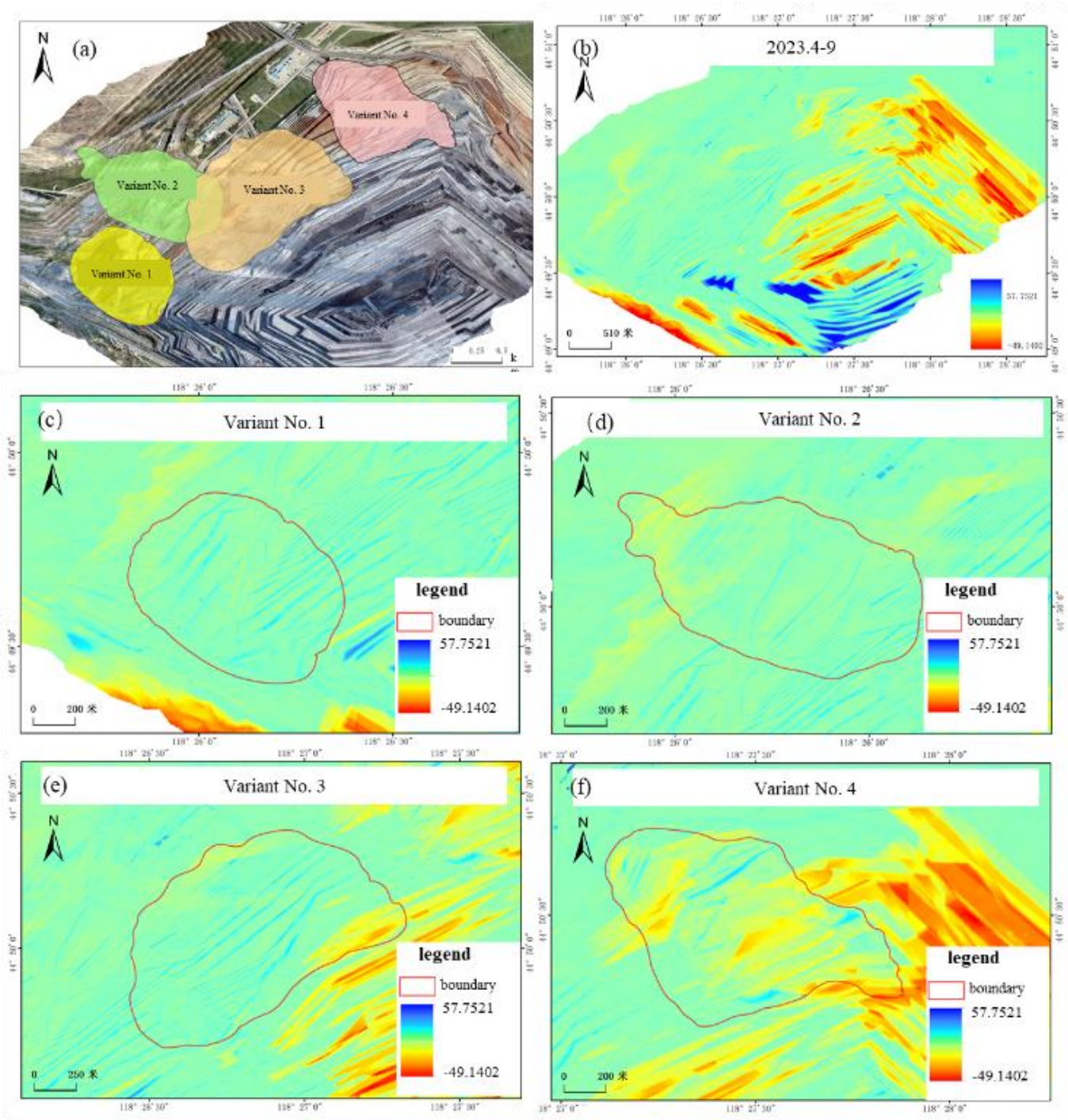

Figure 5: Digital Elevation Model of Difference (DoD) for the four deformation bodies. The calculation period spans 2023.4-9.

5. Discussion

5.1 UAV Photogrammetry for Landslide Monitoring

UAV photogrammetry has increasingly been recognized as an effective tool for landslide mapping and deformation monitoring due to its operational flexibility, high spatial resolution, and cost-efficiency. For instance, Remzi Eker et al. (Eker et al., 2018) applied multi-temporal UAV surveys to monitor the Gallenzerkogel landslide in Austria, achieving vertical RMSE ~4 cm and detecting elevation changes up to ±2.5 m. Similarly, Liu et al. (Lucieer et al., 2014a) demonstrated centimeter-level accuracy for UAV-derived DEMs in Tasmania. These studies corroborate the reliability of our DEM differencing approach.

5.2 Deformation Patterns and Structural Controls

In our case, subsidence concentrated at the midsection and toe aligns with known structural weaknesses (e.g., bedding plane orientation), which is consistent with structural control observed in other settings (e.g., (Niethammer et al., 2012)). The temporal deformation trends across multiple sites further demonstrate that such deformation is progressive and spatially variable—findings echoed in similar multi-temporal landslide investigations.

5.3 Accuracy, Challenges, and Methodological Robustness

Our modeling achieved high geometric accuracy (re-projection error ~0.1 px; RMSE horizontal/vertical within

0.1 m), similar to performance benchmarks in previous UAV studies (Mueller et al., 2016, Du et al., 2018). However, as noted in the literature, UAV-derived DEMs may be subject to terrain artifacts, seasonal vegetation changes, and systematic biases (Szypuła, 2024, Gruszczyński et al., 2021). The use of high overlap, GCPs, and stable calibration in our workflow helps minimize such errors, as recommended in best-practice reviews.

5.4 Implications for Slope Stability Monitoring

The ability to detect deformation at centimeter-scale (and vertical change <0.5 m) provides valuable insight for early detection and risk mitigation in mining slopes (Tsachouridis et al., 2025, Fahle, 2023). Compared to traditional point-based instrumentation, UAV photogrammetry allows full spatial coverage and significant cost savings (~70%)—aligning with findings from other mining deformation studies (Tong et al., 2015). Moreover, the multi-temporal dataset enables the identification of both major and subtle deformation bodies, enhancing understanding of slope evolution (Zhan et al., 2024).

5.5 Recommendations for Future Work

To further improve monitoring capabilities, integrating UAV photogrammetry with complementary techniques—such as LiDAR or InSAR—for enhanced penetration in vegetated areas and continuous deformation tracking is recommended (Sestras et al., 2025, Zhou et al., 2022, Sun et al., 2024). In addition, increasing survey frequency and applying advanced processing methods (e.g., image cross-correlation, machine learning detection) may enhance temporal fidelity and automation.

6. Conclusions

1) Multi-temporal UAV photogrammetry (June and September 2024) using high-resolution optical imaging and precise POS data enabled the generation of orthoimages and DEMs with high geometric fidelity (re-projection error ~0.1 px; GCP-based RMSE: horizontal 0.091 m, vertical 0.080 m).

2) DEM differencing revealed pronounced subsidence (~0.9 m) at the midsection and toe of the primary landslide, while four additional deformation bodies exhibited vertical displacement ranging from 0.2–0.6 m.

Deformation patterns align with structural controls, including bedding and local faults, highlighting the importance of geological context.

3) UAV-based monitoring offers efficient, high-resolution coverage enabling centimeter-to-decimeter displacement detection, with substantial cost reduction (~70%) compared to traditional methods, supporting practical slope stability assessment in mining environments.

4) Future efforts should focus on integrating UAV data with other remote sensing techniques and enhancing temporal resolution to improve monitoring robustness and early warning capabilities.

References

[1] Du D., Qi Y., Yu H., et al. The unmanned aerial vehicle benchmark: Object detection and tracking[C]// Proceedings of the European conference on computer vision (ECCV).2018:370-386.

[2] Eker R., Aydın A., Hübl J. 2018. Unmanned aerial vehicle (UAV)-based monitoring of a landslide: Gallenzerkogel landslide (Ybbs-Lower Austria) case study. Environmental monitoring and assessment [J], 190: 28.

[3] Fahle L. 2023. Mobile Laser Scanning and Octree-Based Statistical Inference Change Detection for Geotechnical Underground Mine Monitoring and Analysis [M]. Colorado School of Mines.

[4] Gruszczyński W., Puniach E., Ćwiąkała P., et al. 2021. Correction of low vegetation impact on UAV-derived point cloud heights with U-Net networks. IEEE Transactions on Geoscience and Remote Sensing [J], 60: 1-18.

[5] James M.R., Robson S., D'oleire-Oltmanns S., et al. 2017. Optimising UAV topographic surveys processed with structure-from-motion: Ground control quality, quantity and bundle adjustment. Geomorphology [J], 280: 51-66.

[6] Kolapo P., Oniyide G.O., Said K.O., et al. 2022. An overview of slope failure in mining operations. Mining [J], 2: 350-384.

[7] Kumari S., Agarwal S., Agrawal N.K., et al. 2025. A comprehensive review of remote sensing technologies for improved geological disaster management. Geological Journal [J], 60: 223-235.

[8] Le Roux R., Sepehri M., Khaksar S., et al. 2025. Slope Stability Monitoring Methods and Technologies for Open-Pit Mining: A Systematic Review. Mining [J], 5: 32.

[9] Lucieer A., Jong S.M.D., Turner D. 2014a. Mapping landslide displacements using Structure from Motion (SfM) and image correlation of multi-temporal UAV photography. Progress in physical geography [J], 38: 97-116.

[10] Lucieer A., Turner D., King D.H., et al. 2014b. Using an Unmanned Aerial Vehicle (UAV) to capture micro-topography of Antarctic moss beds. International Journal of Applied Earth Observation and Geoinformation [J], 27: 53-62.

[11] Mueller M., Smith N., Ghanem B. A benchmark and simulator for UAV tracking[C]//European conference on computer vision. Springer, 2016: 445-461.

[12] Niethammer U., James M., Rothmund S., et al. 2012. UAV-based remote sensing of the Super-Sauze landslide: Evaluation and results. Engineering Geology [J], 128: 2-11.

[13] Sestras P., Badea G., Badea A.C., et al. 2025. A novel method for landslide deformation monitoring by fusing UAV photogrammetry and LiDAR data based on each sensor's mapping advantage in regards to terrain feature. Engineering Geology [J], 346: 107890.

[14] Strzałkowski P., Woźniak J., Górniak-Zimroz J., et al. 2025. Identification and systematics of safety hazards in surface rock mining. Scientific Reports [J], 15: 30492.

[15] Sun J., Yuan G., Song L., et al. 2024. Unmanned aerial vehicles (UAVs) in landslide investigation and monitoring: a review. Drones [J], 8: 30.
[16] Szypuła B. 2024. Accuracy of UAV-based DEMs without ground control points. GeoInformatica [J], 28: 1-28.
[17] Tong X., Liu X., Chen P., et al. 2015. Integration of UAV-based photogrammetry and terrestrial laser scanning for the three-dimensional mapping and monitoring of open-pit mine areas. Remote Sensing [J], 7: 6635-6662.
[18] Tsachouridis S., Pavloudakis F., Sachpazis C., et al. 2025. Monitoring Slope Stability: A Comprehensive Review of UAV Applications in Open-Pit Mining. Land [J], 14: 1193.
[19] Turner D., Lucieer A., Watson C. 2012. An automated technique for generating georectified mosaics from ultra-high resolution unmanned aerial vehicle (UAV) imagery, based on structure from motion (SfM) point clouds. Remote Sensing [J], 4: 1392-1410.
[20] Zhan J., Sun Y., Yu Z., et al. 2024. Characterization of pre-and post-failure deformation and evolution of the Shanyang landslide using multi-temporal remote sensing data. Landslides [J], 21: 1659-1672.
[21] Zhou D., Wang L., An S., et al. 2022. Integration of unmanned aerial vehicle (UAV)-based photogrammetry and InSAR for mining subsidence and parameters inversion: A case study of the Wangjiata Mine, China. Bulletin of Engineering Geology and the Environment [J], 81: 343.